The Cryosphere Discuss., https://doi.org/10.5194/tc-2018-67
Manuscript under review for journal The Cryosphere
Discussion started: 9 April 2018

The Cryosphere
Discussions
Open Access

Cold-to-warm flow regime transition in snow avalanches

Köhler Anselm[1,2], Fischer Jan-Thomas[2], Scandroglio Riccardo[1], Bavay Mathias[1], McElwaine Jim[3], and Sovilla Betty[1]

[1]WSL Institute for Snow and Avalanche Research SLF, Davos Dorf, Switzerland
[2]Austrian Research Centre for Forests (BFW), Innsbruck, Austria
[3]Department of Earth Sciences, Durham University, Durham, UK

Correspondence to: Anselm Köhler, anselm.koehler@slf.ch

Abstract. Large avalanches usually encounter different snow conditions along their track. When they release as slab avalanches comprising cold snow, they can subsequently develop into powder snow avalanches entraining snow as they move down the mountain. Typically, this entrained snow will be cold ($\overline{T} < -1\,°\mathrm{C}$) at high elevations near the surface, but warm ($\overline{T} > -1\,°\mathrm{C}$) at lower elevations or deeper in the snow pack. The intake of thermal energy in the form of warm snow is believed to cause a flow regime transition. Measurements of flow regime transitions are performed at the Vallée de la Sionne avalanche test site in Switzerland using two different radar systems. The data are then combined with snow temperatures calculated with the snow cover model `SNOWPACK`. We define transitions as *complete*, when the deposit at runout is characterized only by warm snow, or as *partial*, if there is a warm flow regime but the furthest deposit is characterized by cold snow. We introduce a transition factor F_t, based on the runout of cold and warm flow regimes, as a measure to quantify the transition type. Finally, we parameterize the snow cover temperature along the avalanche track by the altitude H_s, which represents the point where the average temperature of the uppermost $0.5\,\mathrm{m}$ changes from cold to warm. We find that F_t is related to the snow cover properties, *i.e.* approximately proportional to H_s. Thus, the flow regime in the runout area and the type of transition can be predicted by knowing the snow cover temperature distribution. We find, that, if H_s is more than $500\,\mathrm{m}$ above the valley floor for the path geometry of Vallée de la Sionne, entrainment of warm surface snow leads to a complete flow regime transition and the runout area is reached by only warm flow regimes. Such knowledge is of great importance since the impact pressure and the effectiveness of protection measures are greatly dependent on the flow regime.

1 Introduction

For avalanche practitioners dealing with situations where they need to judge the avalanche hazard for infrastructure, flow regime transitions can cause large uncertainties. Which flow regime reaches the valley bottom is of great interest from two perspectives. Firstly, the usefulness of permanent protection measures like avalanche dams depends strongly on the flow regime (Jóhannesson et al., 2009). Indeed, deflecting and catching dams are relatively ineffective against the highly fluidized intermittent frontal regime of powder snow avalanches, whereas dense flow regimes, especially warm regimes, can be diverted or even stopped. Secondly, the force generated by an avalanche on a structure in the path depends strongly on flow regime (Sovilla et al., 2016).

The dynamic pressure is dominant in cold-dry flow regimes, whereas the hydrostatic contribution is dominant in warm-wet flow regimes.

Recent studies identified the snow temperature as a key parameter causing the agglomeration of snow (Steinkogler et al., 2014) and a change of the flow dynamics by altering the velocity and the effective friction (Naaim et al., 2013; Gauer and Kristensen, 2016), as well as the stopping dynamics (Köhler et al., 2018). A temperature value of -1 °C is proposed by a study on snow granulation (Steinkogler et al., 2015a), where they observed a significant change from millimetre sized grains to the formation of decimetre sized granules above this temperature. We emphasize the temperature of the snow by calling avalanches warm and cold rather than wet and dry, since the flow behaviour changes already at a threshold of -1 °C, when liquid water is still expected to be absent. That this transition occurs below 0 °C is presumably due to the existence of a quasi-liquid layer even at sub-zero temperatures (Dash et al., 2006), which may cause the cohesion of snow to increase.

The avalanche flow regime can be deduced from radar signatures of flow processes by use of the radar GEODAR (Köhler et al., 2018). Cold flow regimes are identified by the starving mechanism in which the avalanche loses mass from the tail until finally the front comes to halt. In contrast, warm flow regimes are identified by either abrupt stopping or a backward propagating shock; either a large flowing part stops instantaneously or the front comes to an halt and incoming material piles up. Köhler et al. (2018) differentiated flow regimes comprising cold and warm snow further in detail. However, relevant for the discussion here is that the majority of large avalanches shows transitions between cold and warm flow regimes. These transitions and the relation with snow cover properties are the focus of this paper.

This study deals exclusively with avalanches that start in a cold-dry regime and later have regions in a warm-wet regime, that is, those avalanches exhibit a cold-to-warm flow regime transition. We define these transitions as *partial transition* or *complete transition*, depending on whether only parts, or the full avalanche, transforms. A partial transition affects only the tail of the flowing avalanche and the final runout is still cold-dominated. With a complete transition, all the snow transforms into warm regimes and the final runout is warm-dominated.

Large avalanches composed mostly of cold snow are powder snow avalanches and have been described by many authors (Sovilla et al., 2015; Issler, 2003; Schweizer et al., 2015). They usually release as a slab containing cold snow, and the runout area is reached by fast flowing cold snow. In addition to the typical structure of a suspension cloud, a frontal intermittent region and a dense tail, GEODAR images reveal often warm flow regimes in the tail and indicate that a partial transition happened (Köhler et al., 2018). Issler (2003) introduced the nomenclature “mixed powder snow avalanche” to describe the occurrence of dilute and dense flow regimes together in one avalanche event. The definition applies mostly for cold dense and dilute regimes, but Issler (2003) reported of damp deposits which are not covered by dust of the dilute regimes and thus had been flowing later and slower.

Warm-dominated avalanches release similarly to cold-dominated ones, but transform completely somewhere along the path. In this case, the runout is dominated by warm regimes. Literature on this type of avalanche is hard to find, since to our knowledge such a transition is rarely recognized and the events are rather described as wet avalanches. There are some measurements with radar and picture in Gauer et al. (2008) indicating a complete transition, but have been interpreted as a secondary wet slab released by the primary dry–cold avalanche. An example of an avalanche with a complete transition released spontaneously near the village of Moos in Passeiertal, Italy, on the 6th of February 2014. A video of this avalanche drew a lot attention, because most of the avalanche travelled along a road in front of houses with people on their balconies (www.youtube.com/watch?v=f5waSw2mMfY). The avalanche released on the south-east facing slopes below the summit of Scheibkopf (2816 m a.s.l.) after a major snow storm and developed a large powder cloud and thus contained cold snow. At around 15 s after the start of the video, the powder cloud began to decay so that the cold parts stopped at approximately 1700 m a.s.l.. A dense flow continued and flowed over a cliff into a shallow valley, where finally a slow-moving plug flow developed. The avalanche transformed completely from a cold powder snow avalanche into a warm flow, which finally flowed slowly along the road.

The present study tries to answer the question of how the *degree* of transition relates to the snow cover properties along the avalanche track. To quantitatively describe the *degree* of transition as a continuum between partial and complete, we define the transition factor F_t, which is a function of the path length of warm and cold flow regimes.

We then explore the relationship with snow cover characteristics, focusing on the snow temperature $\overline{T}$ averaged over the uppermost 0.5 m of the snow cover. This depth is expected to be frequently entrained into the avalanche, though of course there may be more or less entrainment. Despite the crudeness of this measure, we assume that $\overline{T}$ is a representative indicator for the thermal energy intake due to entrainment and we will show that it can be used to give a good prediction of the transition factor.

The study starts by introducing the test site and sensor equipment (sec. 2.1), the method to derive the snow cover temperatures by simulations with the numerical model `SNOWPACK` (sec. 2.2), and a short description of the avalanche data (sec. 2.3). The following results section is divided in two parts. Firstly, we detail the kinematic and dynamic characteristics of partial and complete transitions by means of two different radar systems (sec. 3.1 and 3.2). Secondly, we present the analysis of the degree of transition with the snow cover temperatures (sec. 3.3). Finally, the discussion (sec. 4) brings together both result parts and the study is finished by a conclusion (sec. 5).

2 Methods and data

2.1 Test site and radar sensors

The full-scale avalanche test site Vallée de la Sionne (VdlS) is situated in the west of Switzerland. The east-facing avalanche path extends from high altitudes at 2700 m a.s.l. to intermediate altitudes with a total drop-height of 1300 m. Especially in the early and late season, there can be minimal snow in the lower part of the slope but still sufficient snow for avalanches in the release areas at higher elevations.

The test site is equipped with multiple sensor systems at different locations. On a 20 m high pylon near the start of the runout area, sensors give high-resolution vertical profiles of flow velocity, flow height, density as well as impact pressure (Sovilla et al., 2013). Upward-looking flow profiling radars and seismic sensors are situated in two locations along the flow path. Data are also collected over the entire slope by two complementary radar systems: the GEODAR (Ash et al., 2010) allows tracking of avalanche features with high spatial and temporal resolution, and the pulse-Doppler system (Schreiber et al., 2001) complements this with complete velocity distributions of the avalanche flow. An automatic seismic trigger enables measurement of even spontaneous avalanches.

GEODAR is a high-resolution frequency modulated continuous wave radar and was first installed in winter season 2009/10 (Ash et al., 2014). The system has been continually improved and currently has a range resolution of 0.75 m at 110 Hz over the entire slope (Köhler et al., 2018). GEODAR is able to resolve internal flow structures below the powder cloud. By means of feature tracking, comparison with other data and qualitative interpretations, new and very detailed insights into processes during an avalanche descent have been gained (Vriend et al., 2013; Köhler et al., 2016, 2018). The data processing, feature extraction and terrain registration are done here with the same methods as described in these three publications. An approach velocity $v_a(t)$ of the avalanche front towards the radar is calculated by the derivative of the range-time trajectory $r(t)$, which is corrected for the angle between terrain and the radar beam θ (Köhler et al., 2016)

$$v_a(t) = \frac{\dot{r}(t)}{\cos\theta}\,. \tag{1}$$

The processed GEODAR data are usually shown as range-time plots with the colour representing the intensity of the moving-target identification (MTI) filter (*e.g.* left panels of Fig. 2). This filter suppresses static targets and background clutter and highlights moving structures.

The other radar, a pulse-Doppler radar, was permanently installed at Vallée de la Sionne for the winter season 2009/10 and upgraded in 2016/17. The older system provided a spatial resolution of $R_g = 50$ m and the newer system gives $R_g = 25$ m. This resolution is referred to a range gate extent (R_g), and the Doppler measurements provide an intensity distribution of velocities over time $I_k(t,v)$ of the flowing material within each range gate R_k with a running number k (*e.g.* Fig. 3 and 4). The peak of this distribution describes the velocity of maximum intensity and gives the velocity at which most of the material is travelling (Gauer et al., 2007; Fischer et al., 2014). The data can also be transformed into a range-time representation (Fischer et al., 2016), which is very similar to GEODAR intensity-range plots but represents the mean velocity in each range gate k at each time as

$$\overline{v}_k(t) = \frac{\int v\, I_k(t,v)\, dv}{\int I_k(t,v)\, dv} \tag{2}$$

(middle panels in Figure 2). This can then be converted from a discrete function of range to a continuous function using finite volume interpolation methods.

2.2 Snow cover reconstruction

The test site Vallée de la Sionne is equipped with three weather stations. The bottom station VDS3 (indicated with subscript $_3$) at elevation $H_3 = 1680$ m a.s.l. is representative for the runout area. The top weather station VDS2 (subscript $_2$) at elevation $H_2 = 2390$ m a.s.l. gives a good approximation for the release area even though it is situated 3 km to the north of the avalanche path. Both weather stations are installed in flat fields sheltered from winds to most-accurately represent the undisturbed snow height. Both weather stations measure air temperature, humidity, wind speed, snow height, radiation and snow surface temperature, which are the complete set of parameters necessary to simulate the desired snow cover profiles. A third station VDS1 is situated directly on the ridge above the release area and measures especially wind speed and therefore wind loading.

The Cryosphere Discuss., https://doi.org/10.5194/tc-2018-67
Manuscript under review for journal The Cryosphere
Discussion started: 9 April 2018

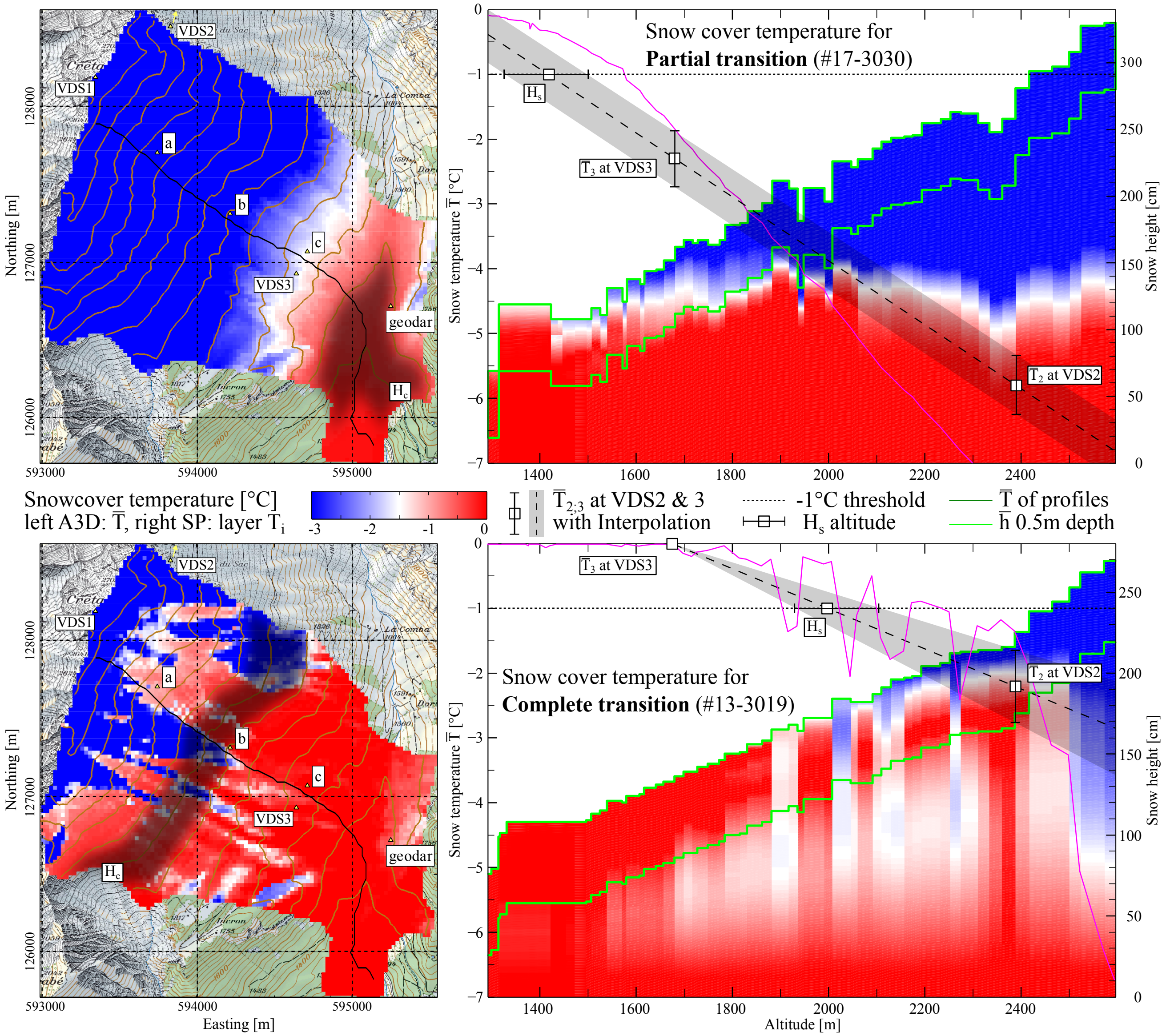

Figure 1. Snow cover simulations for avalanche #17-3030 with partial transition (top) and #13-3019 with complete transition (bottom). The left panels show the $\overline{T}$ values of `Alpine3D` gridded over the VdlS catchment. The area overlay in grey denotes $H_s \pm \triangle H_s$. For reference, the location of the pylon (c) and profiling radars (a, b) are show. The black line indicates the path of steepest descent where the vertical temperature transect in the right panels are evaluated. The purple curve indicate the $\overline{T}$ of each vertical profile. $\overline{T}$ at the top and bottom weather station are shown with squares together with the standard deviation as error. H_s is calculated using linear interpolation between the weather stations and is the intercept of grey area with $-1\,°\mathrm{C}$.

The meteorological data have been prepared with the library `meteoIO` (Bavay and Egger, 2014), *i.e.* missing values have been interpolated and temperature and snow height data have been filtered. Corrections according to Huwald et al. (2009) were necessary for the air temperature, as unventilated temperature sensors are used and these usually overestimate the temperature for situations with low wind speed but strong radiation. Special attention has been given also to the snow height data at the VDS3 station, since for low snow heights the measurements were biased by vegetation so that the values had to be manually reset to $0\,\mathrm{m}$.

To obtain snow temperature profiles, the snow cover has to be modelled as these can not be measured automatically.. The snow cover at the location of the meteo stations has been reconstructed with the numerical energy balance model `SNOWPACK` (Lehning et al., 2002) to obtain vertical snow profiles as a function of time. We have applied the simulation setup for the operational simulations of the Intercantonal Measurement and Information System (IMIS), the high alpine weather station network in Switzerland (Schmucki et al., 2014).

In this publication, we explore how the temperature of the snow cover entering an avalanche determines the degree of a cold-to-warm transition. There is no common approach to reduce the temperature profile of the snow cover to a single representative value. Naaim et al. (2013) used the average snow temperature in the full path without differentiating between release and runout area. This approach is very broad, but suitable for situations where it is necessary to compare a large number of avalanche events. In a detailed study, Steinkogler et al. (2014) averaged over an estimated entrainment depth. This is most accurate but requires very detailed entrainment data, and therefore is only suited for studies with a few avalanches. Köhler et al. (2018) approximated this depth by assuming that the uppermost $0.5\,\mathrm{m}$ of snow was entrained. Sovilla et al. (2006) showed that significant entrainment occurs along the full avalanche path. If we divide the usual total volume of avalanches in VdlS of $(0.5\text{–}1)\times10^6\,\mathrm{m}^3$ by the approximately affected area of $(1\text{–}2)\times10^6\,\mathrm{m}^2$ (Dufour et al., 2000; Steinkogler et al., 2014), the average entrainment depth of $\overline{h}=0.5\,\mathrm{m}$ appears to be a reasonable assumption. The approach with a constant averaging depth can be regarded as a trade-off between accuracy and practicability for analysing many avalanche events, even though large avalanches can usually dig much deeper into the snow cover (Gauer and Issler, 2004; Sovilla et al., 2006).

Thus, we average the simulated snow temperature

$$\overline{T}=\sum_i \frac{h_i T_i}{\overline{h}} \tag{3}$$

from the layers i with thickness h_i and layer temperature T_i in the uppermost $\overline{h}=0.5\,\mathrm{m}$ of the simulated snow cover. With `SNOWPACK` simulations we compute $\overline{T}$ only at the location of VDS2 and VDS3 (squares in right panel of Fig. 1), but are interested in the snow cover temperatures along the entire avalanche path.

We parameterize $\overline{T}$ along the avalanche path with the altitude H_s of the $-1\,^\circ\mathrm{C}$ line. H_s represents the altitude where $\overline{T}$ changes from above to below $-1\,^\circ\mathrm{C}$, similar to the zero-degree level in meteorology. We estimate H_s with a linear relation between the altitude of the weather stations H_2 and H_3 and the average temperatures $\overline{T}_2$ and $\overline{T}_3$ of the uppermost $0.5\,\mathrm{m}$ of the snow cover by

$$H_s=H_b+(H_2-H_3)\frac{-1-\overline{T}_3}{\overline{T}_2-\overline{T}_3}\,. \tag{4}$$

The elevation uncertainty $\triangle H_s$ is estimated with the standard deviation of the uppermost 0.5 m snow temperature $\triangle \overline{T}_{2;3}$ at both weather stations with the law of error propagation. The right panels of Figure 1 show graphically the linear interpolation of $\overline{T}_{2;3}$, and H_s and $\triangle H_s$ is found at the intercept of the grey area with the dashed line at temperature $-1\,°\mathrm{C}$.

Our parameterization of the snow cover temperatures in the avalanche path and the temperature gradient are in fact only dependent on altitude. To check the validity of this strong assumption (Eq. 4), we have additionally performed `Alpine3D` simulations to compare the results (Lehning et al., 2006). `Alpine3D` performs physically-based spatial interpolations of all the meteorological input data over a domain, *i.e.* the area of the VDLS test site. This domain is slit into grid cells with resolution of 25 m x 25 m and for each cell a `SNOWPACK` simulation is performed (Schlögl et al., 2016). While our single `SNOWPACK` simulations are calculated for flat fields, `Alpine3D` simulates the snow cover at each cell with their local slope and aspect. The `Alpine3D` output are grids of a parameter like the 0.5 m snow temperature $\overline{T}$ for every simulation step, and a full `SNOWPACK` output can be generated at any point of interest.

Results of both numerical simulations for two example avalanches are shown in Figure 1. The left panels show the spatial distribution of the $\overline{T}$ temperature over the catchment of VdlS from `Alpine3D`. The right panels display a vertical transect of layer temperatures T_i along the line of steepest descent from the middle of the release area, together with a graphical representation of the interpolation in Eq. 4. These two example avalanches have the largest deviation between Eq. 4 and the `Alpine3D` simulations in our data sets. The #17-3030 event (top) occurred in spring-time when the flat fields receive more sun than the eastern aspects and thus show higher temperature for $\overline{T}_2$ at VDS2 station. The #13-3019 event corresponds to a rain event and the right panel shows isothermal 0 °C snow in the runout area but very cold snow in the release area. However, if compared with the gridded $\overline{T}$ of `Alpine3D` output in the left panels, both H_s estimates (grey areas) reflect reasonably well the warm and cold temperature pattern. Thus, we expect a deviation from equation 4 for situations like spring-time with strong radiation influence, and H_s will be less accurate if large regions are isothermal. In particular, rain-on-snow events may be overlooked as the water ingress is difficult to measure and to capture with `SNOWPACK` (Würzer et al., 2017).

2.3 Data set

In this study, we selected avalanche events from Vallée de la Sionne that fulfil three criteria: 1) they were large enough to pass the measurement pylon at range 655 m near the start of the runout area. This criterion implies an approximate drop height of 1000 m. 2) The avalanche stopped where it was visible to GEODAR, that is before the counter-slope. 3) A cold-to-warm transition as described by Köhler et al. (2018) occurred somewhere in the avalanche.

Since the lower weather station (VDS3) was first employed in the winter season 2012/13, we selected large avalanche events from then until the season 2016/17. From totally measured 130 avalanche events, 18 avalanches fullfil these criteria and were selected. Two of them are compared in detail in Figure 2. The selected avalanches cover the full variability between partial (Sec. 3.1) and complete flow regime transitions (Sec. 3.2). Noteworthy is that avalanches with a complete transition are relatively rare in our data set. There was a three-day period at the beginning of February 2013 when three out of the four of these avalanches occurred. Avalanches with a partial transition could occur all winter from December to March. The avalanche and snow cover data used in this publication are summarized in Table 1.

Table 1. Summary of the avalanche events with the extracted path lengths P, the transition factor $F_t = \frac{P_w - P_c}{\max(P_c, P_w)}$ and altitude of transition H_t, as well as the snowpack conditions H_s and mean temperatures at both meteo stations $\overline{T}_{2;3}$. Data of avalanche events indicated with a * in front of the row can be received from the GEODAR repository (McElwaine* et al., 2017).

SLF-Nr	GEODAR timestamp	P_c [m]	P_w [m]	F_t	H_t [m a.s.l.]	H_s [m a.s.l.]	$\overline{T}_2$ [°C]	$\overline{T}_3$ [°C]
*#13-3003	2012-12-04-04-46-05	1980	1770	-0.11	1820	1719 ± 30	-4.4 ± 0.2	-0.8 ± 0.1
*#13-3019	2013-02-01-17-14-50	1630	2370	0.31	1730	1989 ± 74	-2.3 ± 0.6	0.0 ± 0.0
*#13-3020	2013-02-01-20-18-46	1990	2580	0.23	1660	2003 ± 44	-2.2 ± 0.3	0.0 ± 0.0
*#13-3021	2013-02-02-05-27-31	1560	2230	0.30	1700	1953 ± 26	-2.6 ± 0.2	0.0 ± 0.0
*#13-3024	2013-02-05-23-31-53	2080	1630	-0.22	1770	1506 ± 146	-8.1 ± 1.1	-2.4 ± 1.1
*#14-0012	2014-02-13-19-21-32	2460	1630	-0.34	1770	1325 ± 73	-4.3 ± 0.6	-2.1 ± 0.3
*#15-0009	2015-01-29-05-18-08	1980	1580	-0.20	1810	1627 ± 82	-5.3 ± 0.3	-1.3 ± 0.5
*#15-0013	2015-01-30-02-12-22	2640	1680	-0.36	1810	1200 ± 221	-7.2 ± 0.4	-3.5 ± 0.8
*#15-0016	2015-02-03-10-20-16	2310	1200	-0.48	1870	1281 ± 191	-9.9 ± 0.8	-4.2 ± 1.2
*#15-0020	2015-02-03-12-04-39	2560	1860	-0.27	1770	1585 ± 71	-8.6 ± 0.5	-1.9 ± 0.7
#16-3017	2016-01-18-10-40-14	2640	1370	-0.48	1970	1556 ± 16	-10.4 ± 1.0	-2.4 ± 0.3
#16-3032	2016-02-09-18-31-25	1430	1430	0.00	1960	1858 ± 50	-3.4 ± 0.5	-0.2 ± 0.1
#17-3014	2017-01-13-02-47-38	1760	1560	-0.11	1790	1470 ± 45	-4.5 ± 0.3	-1.8 ± 0.2
#17-3027	2017-03-02-12-22-03	1590	1820	0.13	1820	1979 ± 121	-2.1 ± 0.7	-0.2 ± 0.1
#17-3028	2017-03-06-15-48-07	1990	1530	-0.23	1850	1798 ± 72	-4.0 ± 0.7	-0.4 ± 0.3
#17-3030	2017-03-06-22-05-22	2600	2140	-0.18	1750	1416 ± 77	-5.8 ± 0.5	-2.3 ± 0.4
#17-3033	2017-03-08-11-04-22	2130	2130	0.00	1730	1786 ± 35	-4.4 ± 0.5	-0.4 ± 0.1
#17-3036	2017-03-08-11-25-24	2090	1930	-0.08	1690	1786 ± 35	-4.4 ± 0.5	-0.4 ± 0.1
Moos avalanche, 6 Feb. 2014		1600	2900	0.45	1700	> 2000	–	–

A release location $[X_0, Y_0, Z_0]$ was assigned to each avalanche event by the use of additional data from the VdlS test site as pictures and the flow profiling radars (Köhler et al., 2018). We used a terrain registration procedure to map the radar range onto the line of steepest descent from the release location (*i.e.* green line in Fig. 2). This procedure can be thought of a transfer function between radar range R, real world coordinates $[X, Y, Z]$ and the path length P (Köhler et al., 2016). The path length P is the projected ground parallel distance from the release point $P_0 = 0\,\mathrm{m}$. Since we often do not know precisely the release coordinates, the highest point of the most likely release area was used, giving an uncertainty of $50\,\mathrm{m}$ to $100\,\mathrm{m}$ in path length P.

From the GEODAR MTI plots, we extracted the following ranges and calculated the corresponding path lengths:

- **P_c:** Path length of front containing cold snow, primarily identified by a starving stopping mechanism.
- **P_w:** Path length of front containing warm snow, primarily identified by a backward propagating shock or abrupt stopping.

- **P_t:** Path length until the point of transition between a cold front and a warm front. For avalanches with a complete transition P_t was relatively precise. For partial transitions P_t could be identified only as soon as the warm front separated from the rest of the flow (Fig. 2) and this gave rise to an uncertainty of ± 50 m in path length.

The coloured dots in Figure 2 show the features in the MTI images to which the three points P_c, P_w and P_t belong for two example avalanches. The transfer function between radar range R and path length P is roughly given by the labels in pictures in Figure 2.

3 Results

This section starts with a qualitative characterisation of both cold-to-warm flow regime transition types by means of GEODAR and pulse-Doppler data. Then we relate the degree of transition of all 18 avalanches with the snow cover data. Here, we do not differentiate in detail the flow regimes classified by Köhler et al. (2018), but simply consider cold and warm flow regimes only. We call cold regimes those flow regimes which contain cold snow (< -1 °C), *i.e.* the cold dense regime and intermittent regime. And we call warm regimes those flow regimes which occur for warm snow temperatures (> -1 °C), *i.e.* the warm shear regime and warm plug regime. Warm and cold regimes differ clearly in their MTI stopping signatures. We refer to Köhler et al. (2018) for a detailed description of stopping signatures in the GEODAR signal and the differentiation between cold and warm *flow regimes*.

Figure 2 gives an overview of how cold-to-warm transitions manifest themself in an MTI image, in the mean velocity from Doppler radar and in a picture of the deposit structures. In the pictures, it is feasible to clearly define the deposits of the warm flow regimes (purple and magenta), while the lateral extend of the cold regimes (blue) can only be sketched. The outlines around the flow regimes can also be extracted from the GEODAR and Doppler data (annotated with same colors). Due to a smaller opening angle of the Doppler radar antenna, features on the far-right side of the track are not captured (dashed), but this gives a sort of lateral resolution.

When the deposits which reached the furthest runout distance are cold, a partial transition happend higher up in the avalanche path and deposits of warm snow can be identified (#17-3030, top panels). In contrast, a complete transition happens when an initially cold avalanche starves and transforms into a warm avalanche (#13-3019, bottom panels). Obviously, the velocity of both flow regime types is different. While cold regimes are rather quick, warm flow regimes separate in range and time as they are much slower. The timing when the avalanche reaches the furthest runout distance is therefore different. The avalanche with complete transition (#13-3019) reaches the furthest runout around 350 s later than the avalanche with partial transition (#17-3030).

3.1 Example of a partial transition

The upper panel of Figure 2 shows avalanche #17-3030 as an example of a partial transition. This avalanche originated from the right hand side release area and followed the right couloir. The snow consisted of mainly freshly fallen cold snow and was for most of the avalanche track colder than -1 °C (upper panels of Fig. 1). The -1 °C line was estimated at $H_s =$

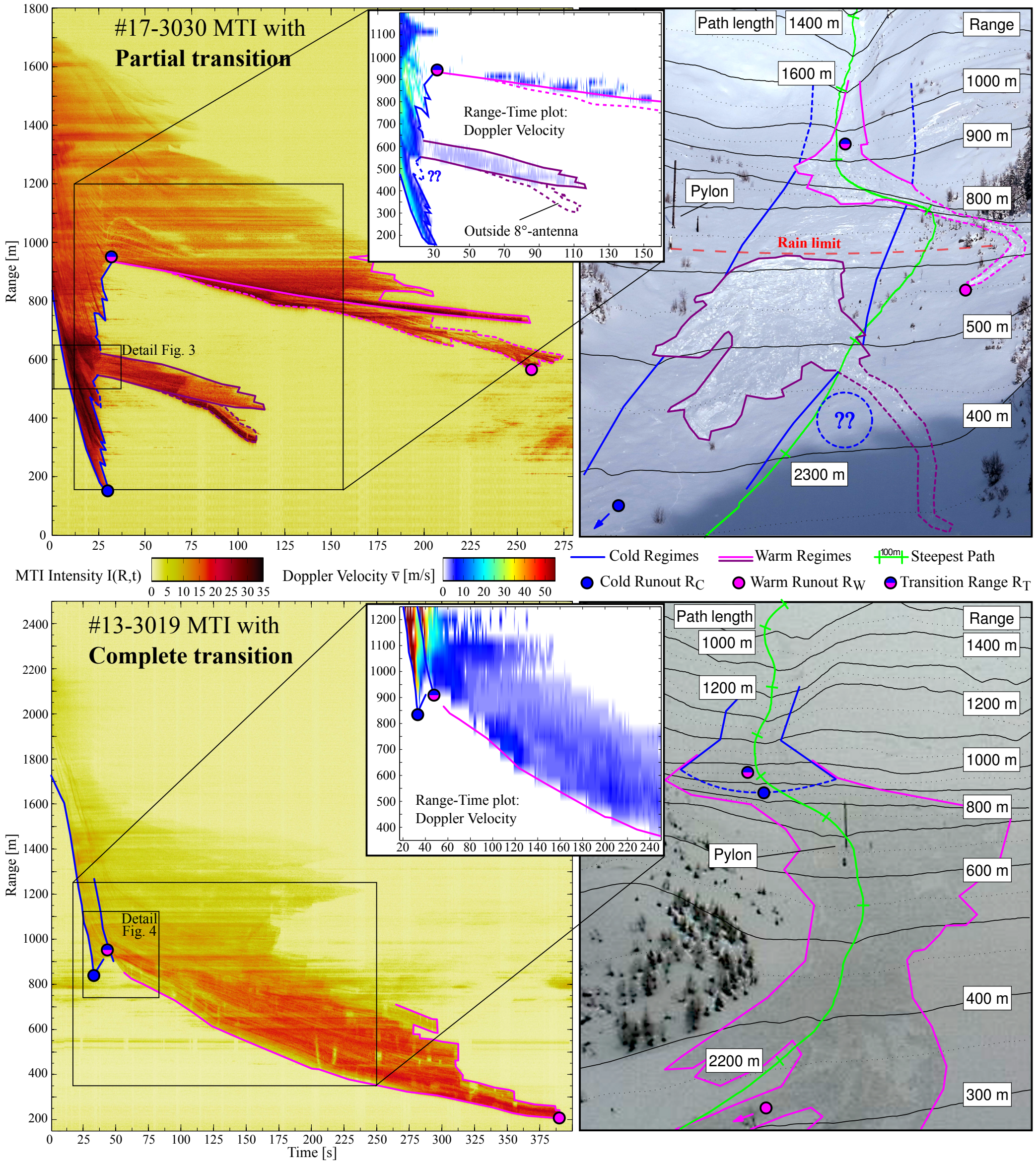

Figure 2. Avalanche examples for a partial (top) and a complete (bottom) cold-to-warm transition. The avalanches are visualized by means of GEODAR data (left), mean Doppler velocities $\overline{v}_k(t)$ (middle) and geo-referenced pictures of the deposits (right). Flow features extracted from GEODAR are highlighted in the other panels. The warm regimes are identified by typical coarse-grained and rough deposits (purple and magenta), while the fine-grained and smooth cold deposits can only be sketched (blue). The path along the steepest descent is drawn in green. The cold and warm runout distances and the transition point are indicated with coloured dots.

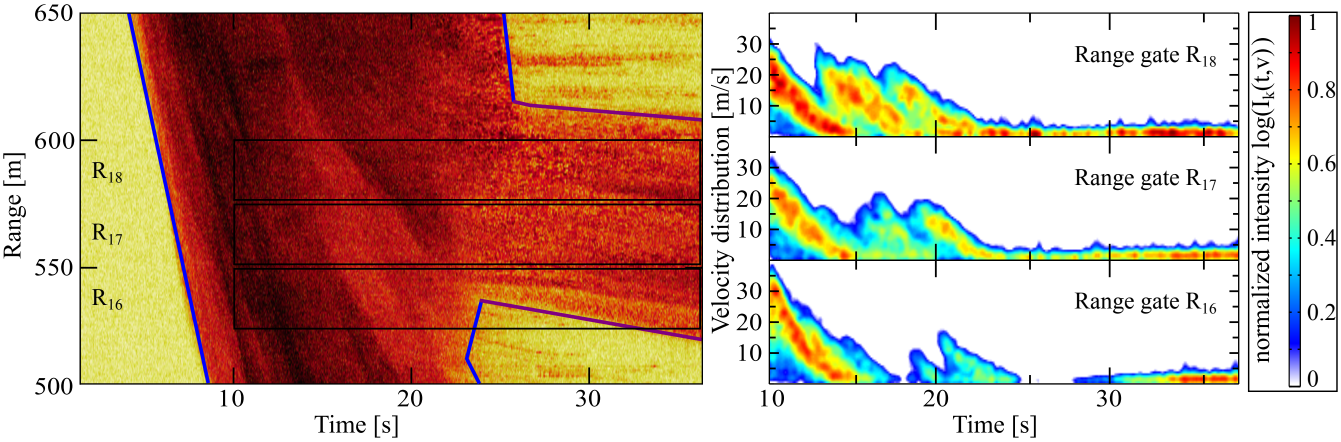

Figure 3. Detail of a partial transition from avalanche #17-3030 from the top panels of Figure 2. Left: Zoomed MTI plot with location of Doppler range gates. Right panels: Doppler velocity distribution in the ranges gates R_{16} (525–550 m), R_{17} (550–575 m) and R_{18} (575–600 m).

(1416 ± 77) m a.s.l. (≈ 200 m range), close to the valley floor and the furthest runout. Avalanche #17-3030 was a typical powder snow avalanche for the Vallée de la Sionne path, with an intermittent regime at the front and followed by a slow moving dense tail (Sovilla et al., 2015). The geo-referenced picture on the top-right of Figure 2 was taken after 1.5 days with intense snow fall. Still, the rough deposition patterns of the warm flow regimes can be easily identified, whereas the fine-grained deposits from the cold flow regimes were hidden under the new snow cover.

The GEODAR data are complemented by velocity data captured by the Doppler radar (top-middle in Fig. 2), which shows the mean velocity $\overline{V}(R,t)$ in a range-time plot, *i.e.* the expected value of the velocity distribution for every time t and range R (Eq. 2). Unfortunately, the start of the Doppler radar was delayed by 10 s, thus most of the front is missing, but the regions inside the avalanche where fast and slower flow regimes prevail can be clearly identified. Several fast surges are visible, and were characterized by a velocity of up to $30\,\mathrm{m\,s^{-1}}$. These surges belonged to the cold regimes which can be identified on the basis of their starving stopping signatures. The furthest point reached by the avalanche was the runout of the cold front at $R_C = 150$ m range (blue dot, Fig. 2, top), which corresponds to $P_c = 2600$ m path length. This avalanche had a cold-dominated runout.

Two slowly flowing tails followed after the front had passed and were characterized by a homogeneous velocity of $2\,\mathrm{m\,s^{-1}}$ to $5\,\mathrm{m\,s^{-1}}$. Both tails show the characteristic abrupt stopping signatures of warm snow. The transition into the magenta tail becomes visible in the MTI plot at the end of the steep couloir at a range $R_T = 950$ m (blue/magenta dot). Interestingly, the avalanche's flowing length started to increase already at a range of 1300 m, which suggests that a transition towards warm and slower regimes may have started higher up. However, the warm tail continued to flow for another 250 s until it finally stopped at $R_W = 550$ m range, corresponding to $P_w = 2140$ m path length. A warm tail like this one is characteristic for most of the powder snow avalanches observed in VdlS.

The tail at 400 m to 600 m range (outlined in dark purple, Fig. 2) is an unusual feature. It originated from entrainment of warm snow in the 20 degree slope of the runout area. Interestingly, the upper boundary of the entrainment corresponds to a rain limit at 1600 m a.s.l. a few days before the avalanche. The liquid water ingress may have caused a weakening of the snow cover.

Figure 3 gives a detail of the transition leading towards this warm tail. In the right panels, the velocity distributions of the corresponding range gates R_{16}, R_{17} and R_{18} from the Doppler radar are shown. Three surges are visible in these range gates with high velocities at their fronts that declines towards their tails. The Doppler data show that the velocity changed during the transition rather gradually from fast to slow. For the first two fronts, the velocity distribution stretches between $10\,\mathrm{m\,s^{-1}}$ to $30\,\mathrm{m\,s^{-1}}$. The lower signal intensity at smaller velocities indicates that most of the snow moves fast. By comparison, the approach velocity of the front v_a extracted from the GEODAR data is around $25\,\mathrm{m\,s^{-1}}$. The third front in R_{18} already contains low velocities at its beginning, possibly corresponding to the formation of the warm tail. The terminal velocity (later than 30 s) of the warm tail is characterised by a narrow velocity distribution as expected for a plug-flow regime.

3.2 Example of a complete transition

The lower panels of Figure 2 show the GEODAR data, Doppler data and a picture of avalanche #13-3019 as an example of a complete cold-to-warm transition. The avalanche descended from left hand side and followed the left couloir. The snow cover was influenced by rain up to around 2000 m a.s.l.. The temperature pattern was highly dependent on the aspect (bottom left of Fig. 1), but the altitude $H_s = (1989 \pm 74)$ m a.s.l. (≈ 1400 m range) visually summarizes the simulated snow cover reasonably well. Avalanche #13-3019 would normally be classified as a warm-wet event, since the deposit showed the typical rough and coarse-grained surface and levées could be identified. But the GEODAR data reveal that a complete flow regime transition occurred at $R_T = 950$ m (magenta/blue dot, bottom left in Fig. 2).

Above R_T, two major surges can be identified with high velocities. The approach velocity v_a measured with GEODAR was $30\,\mathrm{m\,s^{-1}}$ to $35\,\mathrm{m\,s^{-1}}$, while the Doppler data showed mean velocities of $50\,\mathrm{m\,s^{-1}}$ to $60\,\mathrm{m\,s^{-1}}$. This discrepancy corroborates the turbulent character of both surges (Gauer et al., 2007). The first surge continued for another 100 m after the transition point R_T, and finally starved at $R_C = 840$ m range (blue dot, Fig. 2, bottom), corresponding to $P_c = 1630$ m path length.

Below the transition, the avalanche quickly decelerated and revealed the MTI signature of a warm plug regime – the parallel streaks are interpreted as the signature of large granules riding on a fairly stable surface of the flow due to a homogeneous velocity field (Köhler et al., 2018). The mean velocity decreased after the transition to around $3\,\mathrm{m\,s^{-1}}$ to $5\,\mathrm{m\,s^{-1}}$ and was very homogeneous in the full body of the avalanche (bottom-middle in Fig. 2). The warm flow regime continued to flow for another 300 s before reaching the furthest runout at $R_W = 200$ m range (magenta dot) and $P_w = 2370$ m path length. This avalanche thus had a warm-dominated runout.

Figure 4 shows a zoom of the transition region as an MTI image (left) and distributions of the Doppler velocity in three range gates (right). In R_{18}, the front of the first surge showed low intensity for small velocities, but a broad spectrum of velocities between $20\,\mathrm{m\,s^{-1}}$ to $70\,\mathrm{m\,s^{-1}}$. The second surge was in general slower, and showed large intensities in a narrow and slow velocity band. The MTI image indicates that streak signatures (black) crossed the second surge and suggests that

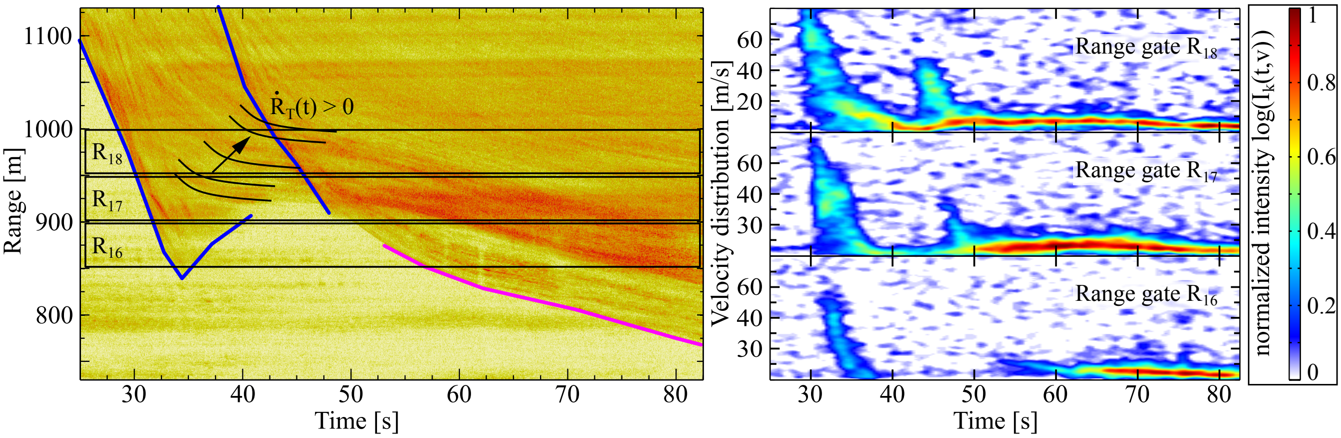

Figure 4. Detail of complete transition from bottom panels of Figure 2. Left: MTI with location of Doppler range gates. The location of transition R_T is not fixed, but moves upward with time $\dot{R}_T(t) > 0$. Right panels: Doppler velocity distribution in range gates R_{16} (850–900 m), R_{17} (900–950 m) and R_{18} (950–1000 m).

the low velocities belonged originally to the first front. The duration of the high velocity region in each surge was rather short with 5 s, compared to fully developed powder snow avalanches where this region can last up to 40 s (Steinkogler et al., 2014). However, the velocity distribution after the transition was narrow with the centre at low and constant velocity indicating a plug flow. Interestingly, the velocity distribution in the plug regime showed very little intensity for velocities between zero and 2–3 m s^{-1}, which indicated a very coherent movement of the avalanche (Fig. 4, Doppler data R_{17} and R_{18} at t > 50 s).

The flow regime transition happened rather quickly in this avalanche, occuring within around 100 m travelled distance and over a period of less than 15 s. Furthermore, the location of the transition seemed to have traveled uphill ($\dot{R}_T(t) > 0$) as the black lines in the left of Fig. 4 indicate. This may be caused by a piling up of incoming fast material on top of the mass of already decelerated material. As in avalanche #17-3030, the flowing length started to increase at a range of 1500 m (bottom-left Fig. 2), indicating a separation of fast and slow material in direction of the flow. Faster and possibly cold material may have been concentrated towards the front, while slower and maybe warm material segregated towards the tail.

3.3 Snow cover influence on transition type

To differentiate between avalanches with partial and complete transitions, we quantify the degree of transition by defining the transition factor

$$F_t = \frac{P_W - P_C}{\max(P_C, P_W)} \tag{5}$$

as the difference between the path length from cold (P_c) and warm (P_w) flow regimes divided by the total path length reached by the avalanche. For avalanches with a partial transition (*e.g.* Sec. 3.1), the transition factor is negative and the runout is dominated by cold regimes. For events with $F_t \approx 0$ the cold regime and the warm regimes reach the same runout. For a positive transition factor, the runout is dominated by warm regimes, corresponding to avalanches with a complete transition

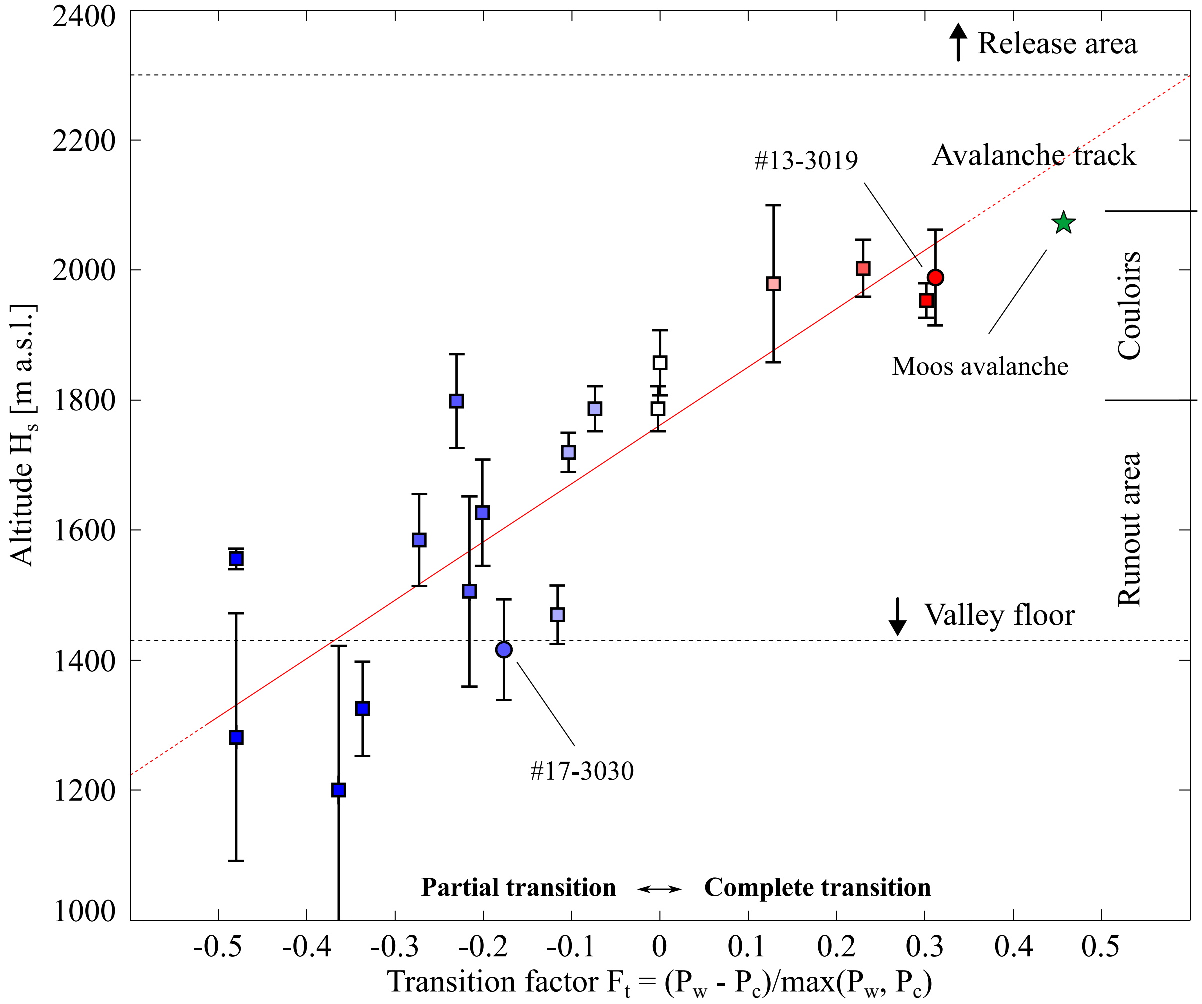

Figure 5. Transition factor F_t as a function of H_s with a linear regression in red. Green star belongs to the Moos avalanche mentioned in the introduction. Horizontal dashed lines and annotation on the right side characterizes roughly the VdlS terrain.

(*e.g.* Sec. 3.2). A value of ± 0.5 means that the dominant regime reaches twice as far as the other regime. The limits of F_t to both sides, *i.e.* $F_t = -1$ and $F_t = 1$, correspond to avalanche types made of purely cold regimes and purely warm regimes, respectively. The avalanches from the examples in Figure 2 have a transition factor of $F_t = -0.18$ (#17-3030) and $F_t = 0.31$ for avalanche #13-3019.

The transition factor F_t together with the altitude H_s for all avalanches are shown in Figure 5. The 18 analysed avalanches cover F_t in the range between -0.5 and 0.4, and all events are well distributed over this range. A linear regression gives $H_s(F_t) = (895 \pm 149) \cdot F_t + (1760 \pm 39)$ with a correlation coefficient of $r = 0.85$. For pure warm avalanches ($F_t = 1$), the regression gives H_s at 2660 m a.s.l., which corresponds to the altitude of the release area. For pure cold avalanches ($F_t = -1$),

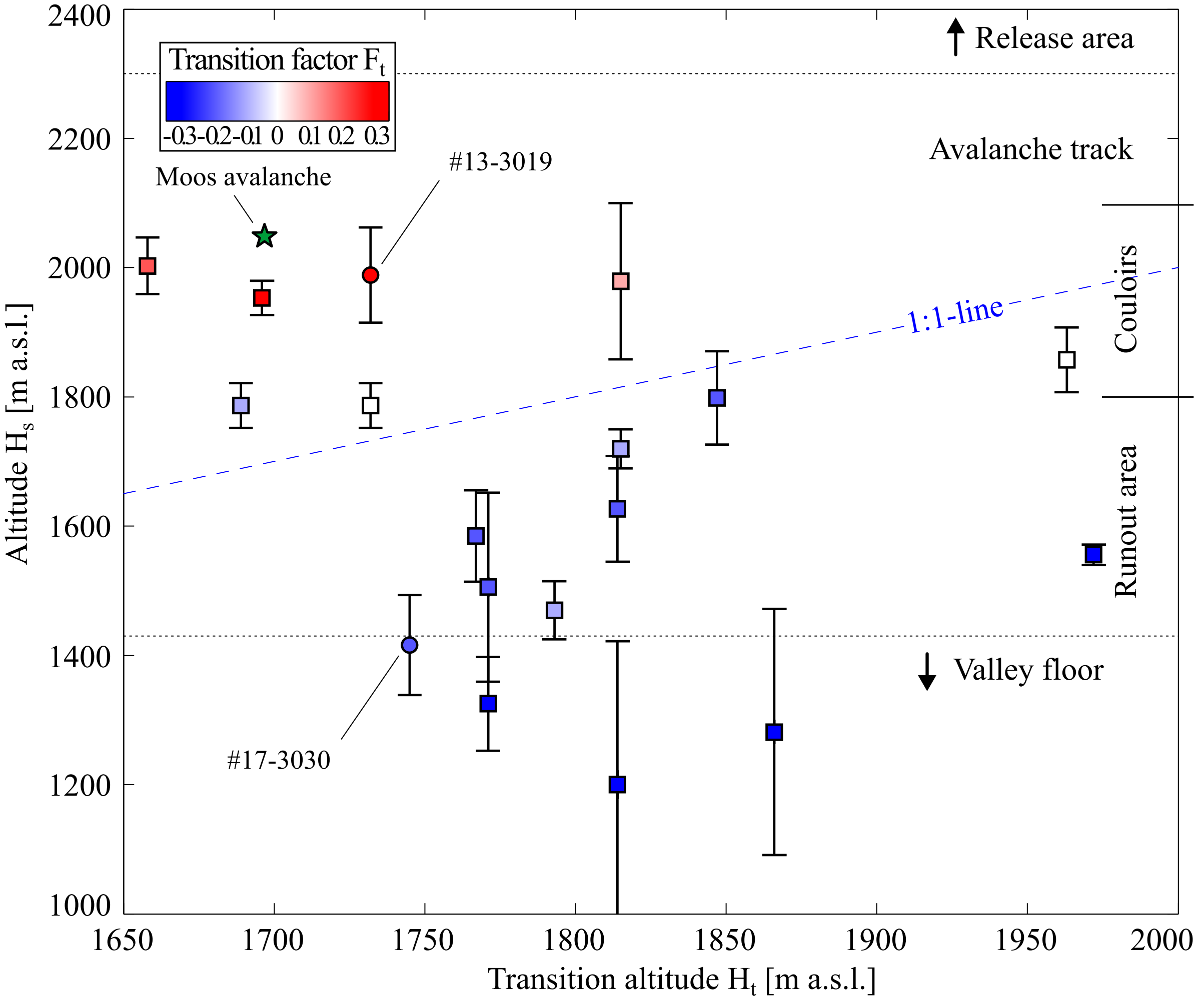

Figure 6. Altitude of transition H_t against the altitude of the $-1\,^\circ$C — line H_s. The 1:1–line (dashed blue) divides the avalanches into cases where the transition happen above or below the H_s-line. Horizontal dashed lines and annotation on the right side characterizes roughly the VdlS terrain. The colour indicate the transition factor from Figure 5.

the regression would give H_s at 860 m a.s.l. which is far below the runout area of Vallée de la Sionne at 1400 m a.s.l. This may indicate that the extrapolation towards purely cold avalanches ($F_t = -1$) has limited validity in this setting.

Figure 6 compares the altitude H_s against the altitude H_t, that is where the snow cover changes from $-1\,^\circ$C against where the transition occurs. We find the altitudes of the transitions H_t scatter on both sides of the 1:1-line (blue dashed); in other words, the transition can happen above or below the H_s-line. Furthermore, H_t can be up to 500 m in elevation away from H_s. The majority of the avalanches perform the transition above the H_s-line, *i.e.* avalanches with a partial transition (blue symbols).

For these events we find that H_s lies below 1700 m a.s.l. and thus in the runout area. And for a few of them, the H_s-line is even below the valley floor (below 1450 m a.s.l.), which in turn means that it can practically not be reached.

The remaining avalanches perform the transition below the H_s, *i.e.* these events express either a complete transition and the warm regimes are dominant in the runout (red symbols), or cold and warm regimes reach similar runouts (white symbols). For these events we find that H_s is consequently higher than 1800 m a.s.l. which corresponds approximately to the altitude of the middle of the avalanche path.

4 Discussion

We find a continuous degree of transition between partial and complete flow regime transitions (Fig. 5). This continuous degree can be related to the altitude H_s, the altitude where the average modelled temperature of the superficial snow layer changes from below to above -1 °C. This means that, for the VdlS avalanche path, the flow regime type in the runout area — but not the runout distance itself — can be estimated when H_s is known.

Avalanches with a cold-dominated runout occur in Vallée de la Sionne when H_s is up to 300 m in elevation above the valley floor. The nomenclature of UNESCO (1981) would classify such an avalanche as “C1G7”, with the code 7 meaning the deposit consists of a mix of cold-dry and warm-wet snow. We find that the point H_t where the transition becomes visible lies exclusively above H_s for cold-dominated avalanches. Thus the transition cannot be caused by snow erosion from the surface, but entrainment of deeper buried and therefore warmer layer of the snow cover must be accounted for. Since the surface (*i.e.* new snow) is cold, a powder snow avalanche maintains its dynamics from surface entrainment, but later flowing parts like the denser core may eventually dig deeper into the snow cover, erode the warmer snow layers and develop a warm tail even above H_s.

We observe that nearly every large powder snow avalanches in Vallée de la Sionne results in a partial transition. This suggests that large purely cold-dry powder snow avalanches are very rare. In all GEODAR data acquired over the last 7 years (140 in total with 20 powder snow avalanches), only one large powder snow avalanche (#15-0017, Köhler et al. (2016)) without a clear partial transition can be found. This avalanche was released shortly after avalanche #15-0016 ($F_t = -0.48$) which had entrained and removed most of the snow in the track. Purely cold-dry avalanches do exist, but perhaps, only as long as they stay small and thus entrain only layers of cold snow close to the surface.

Warm-dominated avalanches are usually classified as wet avalanches, since such a description is mostly based on the deposit structures. Our data show, that initially cold-dry avalanches can lead to complete warm-wet deposits ($F_t > 0$). A special nomenclature for those avalanches does not exist or is not used consistently, even though the UNESCO avalanche classification scheme allows for different wetness classes in the release and runout areas. An avalanche with a complete transition could be denoted as “C1G2” (UNESCO, 1981). The results in Figure 5 indicate that such avalanches occurred in VdlS when H_s is higher than 500 m in altitude above the valley floor. We find that H_t, the point where the transition is initiated, is consequently 200 m to 300 m below H_s (Fig. 6). This indicates that entrainment of warm snow from the surface is most likely the cause for the transition, but also that a previously developed cold flow regime may be able to overflow a surface of warm snow for about

The Cryosphere Discuss., https://doi.org/10.5194/tc-2018-67
Manuscript under review for journal The Cryosphere
Discussion started: 9 April 2018

this distance. As soon as the transition towards warm regimes begins, it happens instantaneously and not gradually, *i.e.* in only 100 m and 15 s (Fig. 4).

Interestingly, the actual altitude of the transition H_t differs for events with partial and complete transitions (Fig. 6). All partial transitions in cold–dominated avalanches occurred in the elevation band between 1750 and 1850 m a.s.l., which corresponds to the altitude of the end of the steep couloir. Complete transitions could occur even at lower elevations down to around 1650 m a.s.l., which correspond to the gentle runout area and even the altitude of the pylon. We think that the above mentioned change in the terrain does not necessarily cause the transition, but gentle terrain may favour the warm and presumably slower flowing snow to separate from fast cold regimes in flow direction. Such a separation can be observed at higher elevations where the flowing length starts to increase and the avalanche extends in range in the MTI plots (Fig. 2). This lengthening occurs most often above H_t and may indicate an earlier start of the transition and a separation of slower and faster flowing regions.

Both transition types are relevant for the dynamics at the avalanche front and especially during deposition in the runout area. For partial transitions, the relevance is indirect as the runout is still cold-dominated, but the slow warm tail is able to hold back mass from the front. For complete transitions the relevance is obvious, as the runout is warm-dominated even though a cold avalanche released. The time-scale when a warm-dominated avalanche reaches the runout is delayed by several hundreds of seconds due to slower velocities of the warm flow regimes (Figure 2). More important, the pressure exerted on structures in the runout depends strongly on the flow regime, and in general is a function of velocity, density and flow height together with a geometry factor (Sovilla et al., 2016). Cold–dominated flow regimes have a dominant velocity squared contribution and the hydrostatic term vanishes due to small densities. In contrast for warm flow regimes, the dynamic term can be neglected due to smaller velocities, but the large density increases the importance of the hydrostatic pressure contribution. Sovilla et al. (2016) presented an example which deviates from the cold or warm pressure scheme and both — dynamic and hydrostatic — contributions are found to be important. We can imagine that avalanches with a complete transition may generate similar high pressures during the transition process as result of remnant high velocities together with an increase in density. Such an argument seems to be different for avalanches with a partial transition. As mentioned above, the warm tail results most likely from deep entrainment by the dense core where the velocities are slower than at the front, so that the dynamic pressure contribution probably stays small.

Another important topic is the extent to which frictional heating due to dissipation processes during the avalanche descent may play a role for flow regime transitions (Vera Valero et al., 2015). Frictional heating compared to a temperature increase due to entrainment was recently investigated experimentally on two medium sized purely cold avalanches by Steinkogler et al. (2015b). They concluded that frictional heating depends mainly on the effective height drop, but the contribution due to entrainment was found to be more variable and dependent on the erosion depth and snow temperature. Here, we cannot differentiate between both heating mechanisms on the basis of our data set. In fact, we include the frictional heating of the flowing snow as it affects P_w and P_c indirectly. However, the relation in Figure 5 indicates that indeed snow erosion and the temperature of the eroded snow have an important effect on the flow dynamics.

Two limitations in regard to temperature exist in our methods. Throughout the whole study, we have assumed that the flowing snow temperature is similar to the snow cover temperature. This is a vague and untested assumption, and the effect depends possibly on the entrainment rate and the temperature difference between the flowing snow and the snow cover. Furthermore, the history of avalanche activity in the avalanche path can significantly alter the snow cover by entrainment and deposition (Steinkogler et al., 2014). The `SNOWPACK` model can account for this with reinitialisation of the snow cover. But this can be only done for artificial avalanches where precise mass-balance measurements are available. Our approach disregards this fact. However, we are interested in the surface layers consisting of the recent new snow precipitation. The simulation of these new top layers is more dependent on the meteorological data than on the older snow layer underneath.

Also questionable appears the estimation of H_s by linear interpolation between two weather stations. We imply that the snow temperature changes only due to an altitude gradient, and this altitude gradient is found to be in the range of $100\,\mathrm{m}\,{}^\circ\mathrm{C}^{-1}$ to $400\,\mathrm{m}\,{}^\circ\mathrm{C}^{-1}$. The estimate of H_s could be improved with detailed analysis performed with distributed snow cover models like `Alpine3D` (Steinkogler et al., 2014). However, we wanted to use a simple parameterization for H_s. “Simple” means that H_s can be estimated from different data sources, *e.g.* field observations or regional snow reports, since for many avalanche paths and past events much less information about the snow cover characteristics is generally available.

Another difficulty is how to generalise our results to other avalanche tracks since we have only investigated a single slope. We expect a path dependence of the correlation between snow cover and the transition factor F_t. Vallée de la Sionne is known to be a relative gentle avalanche path so that avalanches normally stop naturally in the runout area. But for steeper paths, *i.e.* 40° from top to bottom, we expect that more often both flow regimes may reach the valley floor. Our analysis should be extended to take into account other variables, such as volume or mass estimates and path geometry. To directly extend our method to other avalanche paths, regional snow and avalanche reports as well as path length estimation from world-wide available digital terrain models, may already be sufficiently accurate. As example, the Moos avalanche from the introduction fits into the relation found for VdlS (star in Fig. 5 and 6), but noteworthy to say, the geometry of this avalanche path in terms of altitudes, slope and path length, is very similar to the VdlS.

5 Conclusions

GEODAR measurements have shown that flow regime transitions are common large snow avalanches. One of these transitions occur between cold and warm snow when agglomeration of snow crystals cause larger granules to form. In first order, this happens as soon as the flowing snow temperature changes from below to above $-1\,^\circ\mathrm{C}$. Such a flow regime transition is very important for the dynamics of the avalanching snow, as the flow regime influences the pressure exerted on structures in the path. However, we want to stress that the runout distance itself does not depend on the flow regime as cold and warm avalanches can reach unexpected long runouts.

We find two types of cold-to-warm flow regime transitions depending on wether parts or the complete avalanche changes the flow regime. A partial flow regime transition can occur at the tail and depends on the entrainment of deeply buried warm snow layers by the avalanche’s dense core. In contrast, a complete flow regime transition can occur at the front due to the entrainment of warm snow at the surface. We find a continuous degree of transition between both types and a robust relation between this and the snow cover temperature along the avalanche track. More specifically, the transition factor F_t is linearly related to the altitude H_s where the average snow cover temperature in the uppermost 0.5 m changes between warm and cold at a threshold of -1 °C.

At Vallée de la Sionne, almost every large powder snow avalanches exhibit a transition. When H_s is found no higher than 300 m above the valley floor, a partial transition ($F_t < 0$) is observed and results in a warm tail. For complete transitions ($F_t > 0$), the altitude H_s is located more than 500 m above the valley floor and results in only warm flow regimes in the runout area.

This work can be regarded as a step towards the possibility to predict the dominant flow regime in the runout area — but not the runout length — based on knowledge of the snow cover temperature along the path. It is worth mentioning that meteorological and snow cover data from the release area are not representative for the avalanche dynamics in the runout area. Therefore, any hazard and risk evaluation should be made with additional information. Knowing the flow regime in the runout area may improve risk assessment, for example, the effectiveness of a dam may be evaluated in real-time. Nevertheless, the presented approach is strongly dependent on the track geometry and this requires care in adapting our results to other avalanche paths.

Compared to the complexity of temperature influence on avalanche dynamics, our presented method is rather simple. Effects such as frictional heating, temperature difference between entrained and flowing snow, entrainment depth and mixing and separation of snow at differently temperatures are important factors, and to identify their significance on the flow dynamics is a challenging task. We are convinced that future measurement procedures with laser-scans for mass balance, infrared radiation thermography in combination with temperature measurement during the passage of an avalanche, and manual or simulated snow profiles will be very useful to further understand the interplay between these factors. Finally, investigating flow regime transitions in greater detail may become important in respect to climate change. Less snow cover at lower altitudes, strong temperature gradients and quickly varying weather systems may lead to a snow cover situation favouring transitions in avalanches. Warm flow regimes may reach runout areas more frequently and thus require that hazard mitigation procedures are adapted accordingly.

Data availability. The data used in this publication is available upon request to the corresponding author. Most of the GEODAR data can be sourced from the data repository McElwaine* et al. (2017).

Competing interests. The authors declare that they have no conflict of interest.

Acknowledgements. The research was funded by the Swiss National Science Foundation (SNSF) project “High Resolution Radar Imaging of Snow Avalanches,” grant 200021_143435. Special thanks are due to our colleagues at the electronics and workshop of SLF for their invaluable support. We are grateful to Alexander Densmore for his valuable comments on the manuscript.

References

Ash, M., Brennan, P. V., Chetty, K., McElwaine, J. N., and Keylock, C. J.: FMCW Radar Imaging of Avalanche-like Snow Movements, in: Proceedings of the 2010 IEEE Radar Conf., pp. 102–107, IEEE, Arlington, Va., https://doi.org/10.1109/RADAR.2010.5494643, 2010.

Ash, M., Brennan, P. V., Keylock, C. J., Vriend, N. M., McElwaine, J. N., and Sovilla, B.: Two-Dimensional Radar Imaging of Flowing Avalanches, Cold Reg. Sci. Tech., 102, 41–51, https://doi.org/10.1016/j.coldregions.2014.02.004, 2014.

Bavay, M. and Egger, T.: MeteoIO 2.4.2: a preprocessing library for meteorological data, Geosci. Model Dev., 7, 3135–3151, https://doi.org/10.5194/gmd-7-3135-2014, 2014.

Dash, J. G., Rempel, A. W., and Wettlaufer, J. S.: The physics of premelted ice and its geophysical consequences, Rev. Mod. Phys., 78, 695–741, https://doi.org/10.1103/RevModPhys.78.695, 2006.

Dufour, F., Gruber, U., Bartelt, P., and Ammann, W.: Overview of the 1999 measurements at the SLF test site Vallée de la Sionne, in: International Snow Science Workshop, Big Sky–Montana, US, pp. 527–534, 2000.

Fischer, J.-T., Fromm, R., Gauer, P., and Sovilla, B.: Evaluation of probabilistic snow avalanche simulation ensembles with Doppler radar observations, Cold Reg. Sci. Tech., 97, 151–158, https://doi.org/10.1016/j.coldregions.2013.09.011, 2014.

Fischer, J.-T., Köhler, A., Kofler, A., Sovilla, B., and McElwaine, J.: Front and internal velocity distribution in powder snow avalanches, International Snow Science Workshop, Breckenridge, Colorado, 2016.

Gauer, P. and Issler, D.: Possible erosion mechanisms in snow avalanches, Ann. Glaciol., 38, 384–392, https://doi.org/10.3189/172756404781815068, 2004.

Gauer, P. and Kristensen, K.: Four decades of observations from NGI's full-scale avalanche test site Ryggfonn – Summary of experimental results, Cold Reg. Sci. Tech., 125, 162 – 176, https://doi.org/10.1016/j.coldregions.2016.02.009, 2016.

Gauer, P., Kern, M., Krister Kristensen and, Karstein Lied and, L. R., and Schreiber, H.: On pulsed Doppler radar measurements of avalanches and their implication to avalanche dynamics, Cold Reg. Sci. Tech., pp. 55–71, https://doi.org/10.1016/j.coldregions.2007.03.009, 2007.

Gauer, P., Issler, D., Lied, K., Kristensen, K., and Sandersen, F.: On snow avalanche flow regimes: Inferences from observations and measurements, International Snow Science Workshop, Whistler, Canada, pp. 717–723, 2008.

Huwald, H., Higgins, C. W., Boldi, M.-O., Bou-Zeid, E., Lehning, M., and Parlange, M. B.: Albedo effect on radiative errors in air temperature measurements, Water Resour. Res., 45, https://doi.org/10.1029/2008WR007600, w08431, 2009.

Issler, D.: Experimental Information on the Dynamics of Dry-Snow Avalanches, in: Dynamic Response of Granular and Porous Materials under Large and Catastrophic Deformations, edited by Hutter, K. and Kirchner, N., pp. 109–160, Springer, https://doi.org/10.1007/978-3-540-36565-5_4, 2003.

Jóhannesson, T., Gauer, P., Issler, P., Lied, K., Hákonardóttir, K. M., et al.: The design of avalanche protection dams: recent practical and theoretical developments, in: No. EUR 23339 in Climate Change and Natural Hazard Research Series 2, 978-92-79-08885-8, European Commission, 2009.

Köhler, A., McElwaine, J. N., Sovilla, B., Ash, M., and Brennan, P. V.: The dynamics of surges in the 3 February 2015 avalanches in Vallée de la Sionne, J. Geophys. Res., 121, 2192–2210, https://doi.org/10.1002/2016JF003887, 2016.

Köhler, A., McElwaine, J. N., and Sovilla, B.: GEODAR Data and the Flow Regimes of Snow Avalanches, J. Geophys. Res., ??, ??–??, https://doi.org/10.1002/2018J_XXXXXX, 2018.

Lehning, M., Bartelt, P., Brown, B., and Fierz, C.: A physical SNOWPACK model for the Swiss avalanche warning Part III: meteorological forcing, thin layer formation and evaluation, Cold Reg. Sci. Tech., 35, 169–184, https://doi.org/10.1016/S0165-232X(02)00072-1, 2002.

Lehning, M., Völksch, I., Gustafsson, D., Nguyen, T. A., Stähli, M., and Zappa, M.: ALPINE3D: a detailed model of mountain surface processes and its application to snow hydrology, Hydrol. Process., 20, 2111–2128, https://doi.org/10.1002/hyp.6204, 2006.

McElwaine*, J. N., Köhler*, A., Sovilla, B., Ash, M., , and Brennan, P. V.: GEODAR data of snow avalanches at Vallée de la Sionne: Seasons 2010/11, 2011/12, 2012/13 & 2014/15 [Data set], Zenodo, https://doi.org/10.5281/zenodo.1042108, *equally contributing authors, 2017.

Naaim, M., Durand, Y., Eckert, N., and Chambon, G.: Dense avalanche friction coefficients: influence of physical properties of snow, J. Glaciol., 59, 771–782, https://doi.org/10.3189/2013JoG12J205, 2013.

Schlögl, S., Marty, C., Bavay, M., and Lehning, M.: Sensitivity of Alpine3D modeled snow cover to modifications in DEM resolution, station coverage and meteorological input quantities, Environ. Model. Softw., 83, 387 – 396, https://doi.org/10.1016/j.envsoft.2016.02.017, 2016.

Schmucki, E., Marty, C., Fierz, C., and Lehning, M.: Evaluation of modelled snow depth and snow water equivalent at three contrasting sites in Switzerland using SNOWPACK simulations driven by different meteorological data input, Cold Reg. Sci. Tech., 99, 27 – 37, https://doi.org/10.1016/j.coldregions.2013.12.004, 2014.

Schreiber, H., Randeu, W. L., Schaffhauser, H., and Rammer, L.: Avalanche dynamics measurement by pulsed Doppler radar, Ann. Glaciol., 32, 275–280, https://doi.org/10.3189/172756401781819021, 2001.

Schweizer, J., Bartelt, P., and van Herwijnen, A.: Snow Avalanches - Chapter 12, in: Snow and Ice-Related Hazards, Risks and Disasters, edited by Shroder, J. F., Haeberli, W., and Whiteman, C., pp. 395 – 436, Academic Press, Boston, https://doi.org/10.1016/B978-0-12-394849-6.00012-3, 2015.

Sovilla, B., Burlando, P., and Bartelt, P.: Field experiments and numerical modeling of mass entrainment in snow avalanches, J. Geophys. Res., 111, F03007, https://doi.org/10.1029/2005JF000391, 2006.

Sovilla, B., McElwaine, J., Steinkogler, W., Hiller, M., Dufour, F., Suriñach, E., Guillen, C. P., Fischer, J.-T., Thibert, E., and Baroudi, D.: The full-scale avalanche dynamics test site Vallée de la Sionne, International Snow Science Workshop, Grenoble–Chamonix, France, pp. 1350–1357, 2013.

Sovilla, B., McElwaine, J. N., and Louge, M. Y.: The structure of powder snow avalanches, C. R. Phys., 16, 97–104, https://doi.org/10.1016/j.crhy.2014.11.005, 2015.

Sovilla, B., Faug, T., Köhler, A., Baroudi, D., Fischer, J.-T., and Thibert, E.: Gravitational wet avalanche pressure on pylon-like structures, Cold Reg. Sci. Tech., 126, 66–75, https://doi.org/10.1016/j.coldregions.2016.03.002, 2016.

Steinkogler, W., Sovilla, B., and Lehning, M.: Influence of snow cover properties on avalanche dynamics, Cold Reg. Sci. Tech., 97, 121–131, https://doi.org/10.1016/j.coldregions.2013.10.002, 2014.

Steinkogler, W., Gaume, J., Löwe, H., Sovilla, B., and Lehning, M.: Granulation of snow: From tumbler experiments to discrete element simulations, J. Geophys. Res., 120, 1107–1126, https://doi.org/10.1002/2014JF003294, 2015a.

Steinkogler, W., Sovilla, B., and Lehning, M.: Thermal energy in dry snow avalanches, Cryosphere, 9, 1819–1830, https://doi.org/10.5194/tc-9-1819-2015, 2015b.

UNESCO: Avalanche atlas: Illustrated international avalanche classification, Tech. rep., International Commission on Snow and Ice, UNESCO, Paris, http://unesdoc.unesco.org/Ulis/cgi-bin/ulis.pl?catno=48004&gp=1&lin=1&ll=1, 1981.

Vera Valero, C., Wikstroem Jones, K., Bühler, Y., and Bartelt, P.: Release temperature, snow-cover entrainment and the thermal flow regime of snow avalanches, J. Glaciol., 61, 173–184, https://doi.org/10.3189/2015JoG14J117, 2015.

Vriend, N. M., McElwaine, J. N., Sovilla, B., Keylock, C. J., Ash, M., and Brennan, P. V.: High-resolution Radar Measurements of Snow Avalanches, Geophys. Res. Lett., 40, 727–731, https://doi.org/10.1002/grl.50134, 2013.

Würzer, S., Wever, N., Juras, R., Lehning, M., and Jonas, T.: Modelling liquid water transport in snow under rain-on-snow conditions - considering preferential flow, Hydrol. Earth Syst. Sci., 21, 1741–1756, https://doi.org/10.5194/hess-21-1741-2017, 2017.